© 2020. Published by The Company of Biologists Ltd | Development (2020) 147, dev189241. doi:10.1242/dev.189241

RESEARCH REPORT

Disruption of the nectin-afadin complex recapitulates features of the human cleft lip/palate syndrome CLPED1

Kendall J. Lough[1], Danielle C. Spitzer[1,*], Abby J. Bergman[1,†], Jessica J. Wu[1], Kevin M. Byrd[1,2] and Scott E. Williams[1,‡]

ABSTRACT

Cleft palate (CP), one of the most common congenital conditions, arises from failures in secondary palatogenesis during embryonic development. Several human genetic syndromes featuring CP and ectodermal dysplasia have been linked to mutations in genes regulating cell-cell adhesion, yet mouse models have largely failed to recapitulate these findings. Here, we use *in utero* lentiviral-mediated genetic approaches in mice to provide the first direct evidence that the nectin-afadin axis is essential for proper palate shelf elevation and fusion. Using this technique, we demonstrate that palatal epithelial conditional loss of afadin (*Afdn*) – an obligate nectin- and actin-binding protein – induces a high penetrance of CP, not observed when *Afdn* is targeted later using *Krt14-Cre*. We implicate *Nectin1* and *Nectin4* as being crucially involved, as loss of either induces a low penetrance of mild palate closure defects, while loss of both causes severe CP with a frequency similar to *Afdn* loss. Finally, expression of the human disease mutant *NECTIN1*^{W185X} causes CP with greater penetrance than *Nectin1* loss, suggesting this alteration may drive CP via a dominant interfering mechanism.

KEY WORDS: Palatogenesis, Cleft palate, Afadin, Nectin, CLPED1

INTRODUCTION

Orofacial clefting is a common congenital defect affecting nearly 200,000 infants each year. These frequently-monogenetic developmental malformations usually include cleft lip and/or cleft palate (CP), occurring alone or as part of a syndrome. Cleft lip/palate-ectodermal dysplasia syndrome 1 (CLPED1; OMIM #225060) – also known as orofacial cleft 7 (OFC7), Zlotogora-Ogur syndrome and Margarita Island ectodermal dysplasia (ED4) – was originally identified as a recessive disorder affecting isolated populations in the Middle East, South America and the Caribbean (Bustos et al., 1991; Rodini and Richieri-Costa, 1990; Zlotogora, 1994; Zlotogora and Ogur, 1988). Homozygous mutations in *NECTIN1* that truncate the receptor within its extracellular domain at Trp185 were identified in two families with CLPED1 (Suzuki et al., 2000); however, mouse models of *Nectin1* loss do not appear to cause CP or ED (Barron et al., 2008; Inagaki et al., 2005; Yoshida et al., 2010).

[1]Departments of Pathology & Laboratory Medicine and Biology, Lineberger Comprehensive Cancer Center, The University of North Carolina, Chapel Hill, NC 27599, USA. [2]Department of Oral & Craniofacial Health Sciences, The University of North Carolina School of Dentistry, Chapel Hill, NC 27599, USA.
*Present address: Molecular and Cellular Biology Program, University of California, Berkeley, Berkeley, CA 94720, USA †Present address: Department of Genetics, Stanford University, Palo Alto, CA 94305, USA

‡Author for correspondence (scott_williams@med.unc.edu)

K.J.L., 0000-0001-9663-6983; D.C.S., 0000-0003-4827-1857; S.E.W., 0000-0001-9975-7334

Received 10 February 2020; Accepted 2 June 2020

With its similarity to human craniofacial development and genetic malleability, the mouse is an excellent model for studying palatogenesis (Bush and Jiang, 2012). There are ∼50 genes linked to orofacial clefting in humans and >100 in mice, and many of these are orthologs (Dixon et al., 2011). In murine palatogenesis, palatal shelves (PSs) emerge at E11.5, extend downward between E12 and E13.5, rapidly elevate over the tongue at ∼E14, and elongate horizontally, fusing along the midline by E15.5 (Bush and Jiang, 2012; Greene and Pratt, 1976; Walker and Fraser, 1956). PSs are lined by a bilayered epithelium consisting of basal cells overlaid with protective periderm, which prevents the formation of intraoral adhesions between juxtaposed epithelia, such as the PS and tongue (Hammond et al., 2019; Richardson et al., 2009). As they approach the midline, opposing PS epithelia adopt an adhesive-competent identity as the medial edge epithelia (MEE). They form the midline (medial) epithelial seam (MES) during fusion, with residual epithelial cells removed through a combination of migration, apoptosis and differentiation (Hammond et al., 2019; Kim et al., 2015). Failure at any step can result in CP, perhaps explaining its high incidence and genetic heterogeneity (Dixon et al., 2011; Kousa et al., 2017; Mossey et al., 2009).

Nectins are transmembrane cell-cell adhesion proteins – consisting of four members in mice and humans – that homodimerize in *cis* and generally heterotetramerize in *trans* (Momose et al., 2002; Yasumi et al., 2003). Different nectin homodimers interact in *trans* with variable affinity; e.g. nectin 1 preferentially binds to nectin 3 and nectin 4 (Reymond et al., 2001). This hierarchical binding affords the nectins cell sorting functionality, as demonstrated in the olfactory epithelia and cochlea (Katsunuma et al., 2016; Togashi et al., 2011). The nectin cytoplasmic tail forms an obligate interaction with the actin-binding protein afadin, which links the cytoskeleton to the adherens junction (AJ) (Mandai et al., 1997; Miyahara et al., 2000; Takahashi et al., 1999).

Recent work suggests that an interaction between nectin 1 and nectin 4 may be important for palatogenesis (Mollo et al., 2015; Richardson et al., 2017). Interestingly, mutations in *NECTIN4* underlie a related developmental disorder, ectodermal dysplasia syndactyly syndrome (EDSS1; OMIM #613573) (Brancati et al., 2010). However, *Nectin4* loss has not been modeled in mice, so its role in palatogenesis remains unknown. Here, using a versatile *in utero* lentiviral genetic toolkit, we provide the first functional evidence that the nectin-afadin cell-adhesion complex is required for proper palate closure. Furthermore, we demonstrate that *Nectin1* and *Nectin4* act cooperatively during palatogenesis, and that human CLPED1 mutations induce CP and syndactyly in mice through a dominant-interfering mechanism.

RESULTS AND DISCUSSION

Afadin is required for secondary palatogenesis

To generate a model of pan-nectin loss, we targeted the obligate nectin binding partner afadin. As germline afadin (*Afdn*) knockouts

Development (2020) 147, dev189241. doi:10.1242/dev.189241

are non-viable (Ikeda et al., 1999; Zhadanov et al., 1999), we used a well-characterized *in utero*, lentiviral-based genetic manipulation technique to generate conditional epithelial loss-of-function embryos (Beronja et al., 2010). This LUGGIGE (lentiviral ultrasound-guided gene inactivation and/or gene expression) approach can achieve ∼50-70% transduction of palatal epithelium (Beronja et al., 2010; Byrd et al., 2016; Lough et al., 2017). Moreover, LUGGIGE delivery of Cre recombinase at E9.5 drives reporter gene expression by E10.5, 2-3 days earlier than a commonly used transgenic *Krt14-Cre* line (Beronja et al., 2010). A similar approach using adenovirus demonstrated that periderm-specific re-expression of TGFβ3 rescued CP in *Tgfb3* knockouts (Wu et al., 2013). Thus, *in utero* delivery of viral vectors represents a powerful and versatile approach to genetically manipulate oral epithelia during palatogenesis, offering several advantages over traditional transgenics (Lough et al., 2017).

We used LUGGIGE to generate two tissue-specific *Afdn* loss-of-function models (Fig. 1A): (1) knockdown with a previously validated *Afdn*^{2711} shRNA (Lough et al., 2019); (2) knockout using RFP-tagged Cre recombinase injected into *Afdn*$^{fl/fl}$ mice (Beaudoin et al., 2012). For the first strategy, we injected E9.5 CD1 mice with lentivirus harboring the *Afdn*^{2711} shRNA and an mRFP1 fluorescent reporter fused to histone-2B (H2B-mRFP1) (Fig. 1A). RFP+ and wild-type, uninjected littermates were collected at various timepoints to evaluate palatogenesis and validate shRNA efficiency (Fig. 1B). *Afdn*^{2711} embryos displayed near-complete loss of afadin accumulation in palatal epithelia by E14.5 (Fig. S1A). Although CP in wild-type littermates was rare (1/16; 4 litters), most *Afdn*^{2711} embryos (13/17; 4 litters) presented with severe CP (Fig. 1C,D). Importantly, neither a *Scramble* non-targeting shRNA (n=10; 5 litters) nor empty vector H2B-mRFP1 control (n=4) caused CP when evaluated in the same manner (Fig. 1D; Fig. S1B).

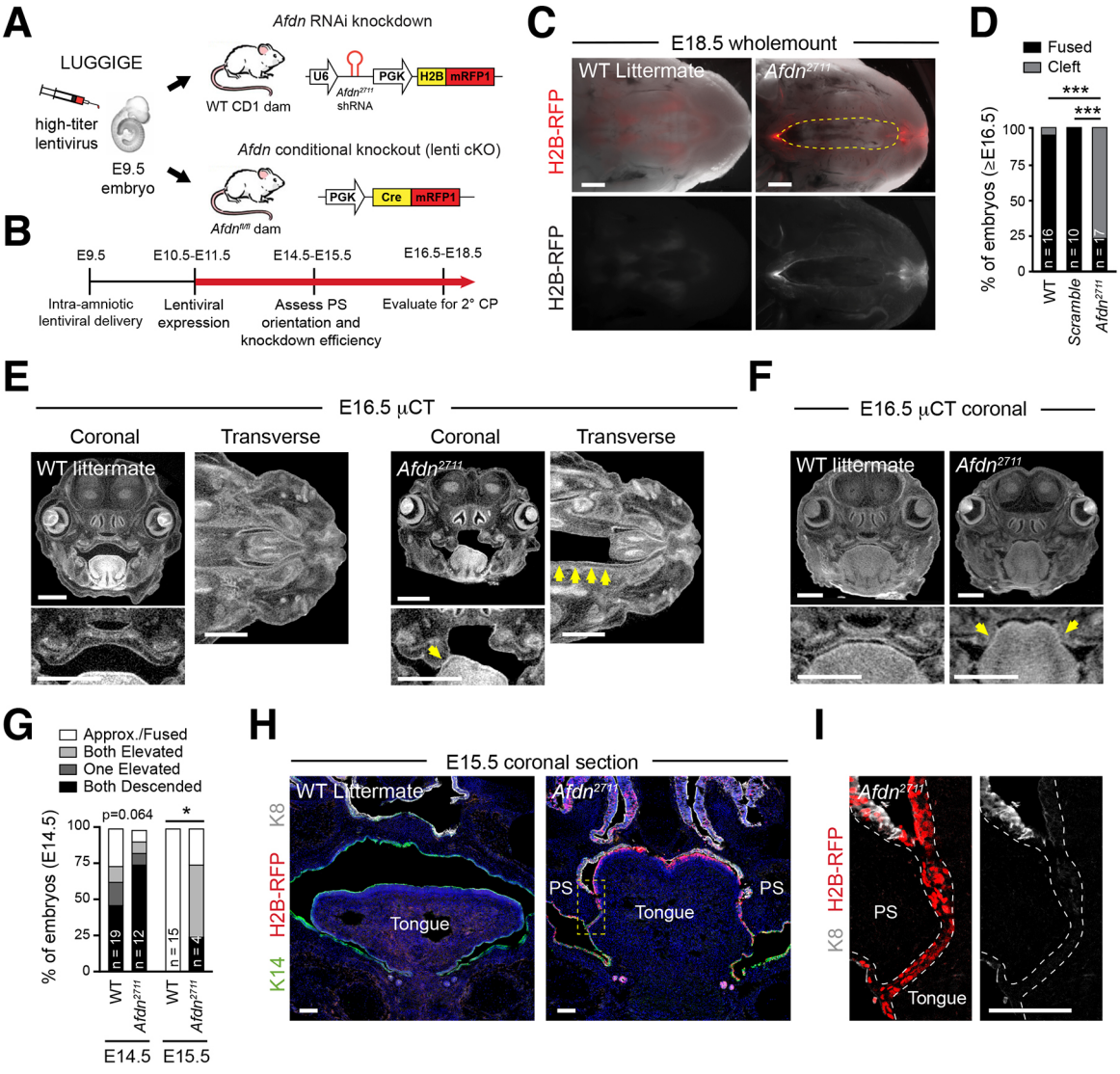

Fig. 1. Afadin is essential for secondary palatogenesis. (A) LUGGIGE experimental approach. (B) Timeline of LUGGIGE and experimental endpoints. (C) Dark-field (top) and fluorescent (bottom) stereoscope images of E18.5 *Afdn*^{2711} infected embryo and uninjected littermate. H2B-RFP (red) is overlaid in the top panel. *Afdn*^{2711} embryos consistently present with CP (yellow outline). (D) CP frequency in *Afdn*^{2711} embryos, wild-type littermates and scramble controls. (E,F) Contrast-enhanced µCT images of E16.5 *Afdn*^{2711} and littermate heads. *Afdn* knockdown embryos frequently display with one (E) or both (F) PS still descended (yellow arrows). (G) Quantification of PS elevation phenotypes at E14.5 and E15.5 in *Afdn*^{2711} and wild-type littermates. (H) E15.5 *Afdn*^{2711} and wild-type coronal sections immunostained with K14 (green), K8 (grey) and lentiviral H2B-RFP (red). (I) Detailed view of the dashed box in H showing a region of intraoral adhesion between PS and tongue epithelia. Scale bars: 1 mm in C,E,F; 100 µm in H,I. *P<0.05, ***P<0.001 (Fisher's exact test).

Development (2020) 147, dev189241. doi:10.1242/dev.189241

We developed a novel contrast-enhanced μCT technique which allows non-invasive visualization of the embryonic palate at 6 μm resolution in three dimensions (see Materials and Methods) (Fig. 1E,F). Using this technique, plus serial cryosectioning and immunofluorescence, we demonstrated that E16.5 *Afdn*^{2711} embryos display a variety of defects in both PS elevation and fusion (Fig. 1E,F; Fig. S1C). These diverse phenotypes could be attributable to differences in transduction efficiency or the inherent variability in the progression of palatogenesis between littermates. However, in nearly all cases, the PS remained in direct contact with the tongue, a hallmark of persistent intraoral adhesions. We next examined earlier timepoints and observed that *Afdn*^{2711} embryos displayed delays in shelf elevation between E14.5-E15.5 (Fig. 1G,H). Interestingly, E15.5 *Afdn*^{2711} knockdown animals with near-complete lentiviral transduction frequently presented with descended PS, which appeared to lack a K8-positive periderm layer between palatal and tongue epithelia (Fig. 1I). Thus, afadin loss could induce CP by delaying palatal shelf elevation, which may cause – or be attributed to – the formation of intraoral adhesions.

LUGGIGE-mediated Cre presents advantages over epithelial-specific Cre transgenics

We next created conditional knockouts using LUGGIGE to deliver Cre-RFP into homozygous *Afdn*$^{fl/fl}$ embryos (hereafter referred to as *Afdn* lenti-cKO). Like *Afdn*^{2711} embryos, nearly all E16.5 *Afdn* lenti-cKO mutants displayed CP (4/5 embryos; two litters) (Fig. S1D,E). Interestingly, however, epithelial-specific *Krt14-Cre; Afdn*$^{fl/fl}$ conditional knockout embryos never displayed CP (0/17 embryos; three litters) (Fig. S1D). We attribute this discrepancy to differences in the timing of Cre activation because *Afdn* lenti-cKOs display complete loss of afadin immunostaining in E13.5 PS whereas *Krt14-Cre*; *Afdn*$^{fl/fl}$ embryos still show residual protein (Fig. S1F). This highlights potential concerns in using some *Krt14-Cre* strains because recombination may not occur early enough. However, other *Krt14-Cre* lines (Andl et al., 2004; Vasioukhin et al., 1999) have been used to generate CP models, suggesting that differences in the timing and/or expression of Cre recombinase must be considered (Lough et al., 2017). Nonetheless, LUGGIGE circumvents this issue because it drives epithelial-specific expression from early stages of palatogenesis.

Epithelial loss of *Nectin1* or *Nectin4* results in mild low-penetrance CP

Despite the well-characterized link between *NECTIN1* and *NECTIN4* mutations with CP and ED, mouse models have failed to recapitulate these phenotypes. CP has not been reported in any *Nectin1*, *Nectin2* or *Nectin3* single mutant or in compound mutants where three Nectin alleles are deleted (Bouchard et al., 2000; Inagaki et al., 2005; Yoshida et al., 2010). In addition to nectin 1 and nectin 2, nectin 4 is also expressed in the MEE (Richardson et al., 2017; Yoshida et al., 2012), but the consequence of *Nectin4* loss has not been explored.

Because 'transcriptional adaptation' can lead to compensatory upregulation of related genes in germline knockouts (El-Brolosy et al., 2019), we re-evaluated the role of *Nectin1* and *Nectin4* in palatogenesis using LUGGIGE-mediated knockdown. To do so, we screened panels of shRNAs in cultured keratinocytes via RT-qPCR and chose two for each gene with the highest knockdown efficiencies (see Materials and Methods). As a direct readout of shRNA efficacy, we performed immunofluorescent staining in cultured keratinocytes, which demonstrated robust loss of target protein accumulation (Fig. S2).

Nectin 1 and nectin 4 localize to the interface between palatal basal cells and periderm at E13.5 (Richardson et al., 2017). Whereas *Nectin1* is a direct target of the basal-specific transcription factor p63 (*Trp63*) in both epidermis and palatal epithelium – and is lost in *Trp63* knockouts – *Nectin4* is regulated by Irf6, and is still expressed in *Trp63* knockouts (Ferone et al., 2012; Mollo et al., 2015; Richardson et al., 2017). The fact that *Nectin1* and *Nectin4* are subject to distinct modes of transcriptional regulation suggests they may be expressed in different cell populations. In support of this, single-cell RNA-Seq data show that *Nectin4* is highly enriched in periderm while largely absent from palatal epithelium (Li et al., 2019). Because LUGGIGE achieves mosaic transduction, it can be used to resolve which cell layers express nectin 1 and nectin 4. At E14.5, *Nectin1* loss in RFP+ basal cells, but not periderm, was sufficient to ablate nectin 1 staining, while *Nectin4* loss in RFP+ periderm achieved nectin 4 protein loss at this interface (Fig. 2A-C). These data suggest that nectin 1 is specifically expressed by basal cells while nectin 4 is predominantly expressed in periderm.

We next examined the requirement of nectin 1 and nectin 4 in palatogenesis using LUGGIGE (Fig. 2D-F). Both *Nectin1* and *Nectin4* loss resulted in CP, albeit with low penetrance (11% for *Nectin1*^{4402}; 40% for *Nectin1*^{2732}; 20% for *Nectin4*^{2589} and *Nectin4*^{2632}). Notably, the phenotype was also less severe than *Afdn* loss-of-function embryos. Finally, while *Nectin1* knockdown caused uniform clefting of the secondary palate region, *Nectin4* knockdown frequently resulted in posterior-specific CP (Fig. 2D).

Dual loss of *Nectin1* and *Nectin4* causes highly penetrant cleft palate

To test whether multiple nectins cooperate to promote palate closure, we first co-injected two lentiviruses targeting *Nectin1*^{4402} and *Nectin4*^{2589}, each with distinct fluorescent reporters (Fig. 3A). This pooled approach resulted in a higher penetrance of CP (3/7 embryos; 3 litters) compared with loss of only one nectin (Fig. 3B,C). Furthermore, two additional embryos presented with a posterior submucosal cleft (SMC). Although this approach increased CP incidence, it could underestimate the effect of combined loss of *Nectin1* and *Nectin4*, as RFP/YFP double-positive cells were rare (Fig. S3A). We therefore generated a new lentiviral construct that allowed for simultaneous expression of multiple shRNAs with a single H2B-mRFP1 reporter by adding an H1 promoter driving *Nectin4*^{2589} shRNA expression upstream of the original U6 promoter-*Nectin1*^{4402} shRNA cassette (Fig. 3D; hereafter referred to as *N1*^{4402}*; N4*^{2589}). By E14.5, *N1*^{4402}*; N4*^{2589} RFP+ palatal epithelium displayed efficient loss of both nectin 1 and nectin 4 (Fig. S3B), and at E16.5, nearly all RFP+ embryos displayed CP (11/12 embryos; three litters; Fig. 3E,F). Additionally, in the one *N1*^{4402}*; N4*^{2589} RFP+ embryo without obvious CP, we observed persistent K14+ epithelial cells within the palatal mesenchyme, indicating a failure to complete MES dissolution (Fig. S3C). Looking earlier, at E14.5, *N1*^{4402}*; N4*^{2589} embryos were more likely to have both shelves still descended compared to wild-type littermates (Fig. 3G; Fig. S3D). By E15.5, when wild-type littermates had largely completed palatogenesis (9/10 embryos; 2 litters), half of *N1*^{4402}*; N4*^{2589} embryos displayed an unusual phenotype where only one PS elevated (Fig. 3G,H). Although not as dramatic as in *Afdn* knockdowns, we observed direct contact between the PS and lateral tongue in E14.5 *N1*^{4402}; *N4*^{2589} embryos, with similar gaps in K8+ periderm coverage (Fig. S3E). This suggests that *Nectin1* and *Nectin4*, acting through *Afdn*, promote PS elevation, possibly by preventing aberrant intraoral adhesions.

Causal CLPED1 mutations drive CP via dominant interfering activity

Mutations in *NECTIN1* have been implicated as casual variants for CLPED1 (Suzuki et al., 2000). Most *NECTIN1* alterations are nonsense

Development (2020) 147, dev189241. doi:10.1242/dev.189241

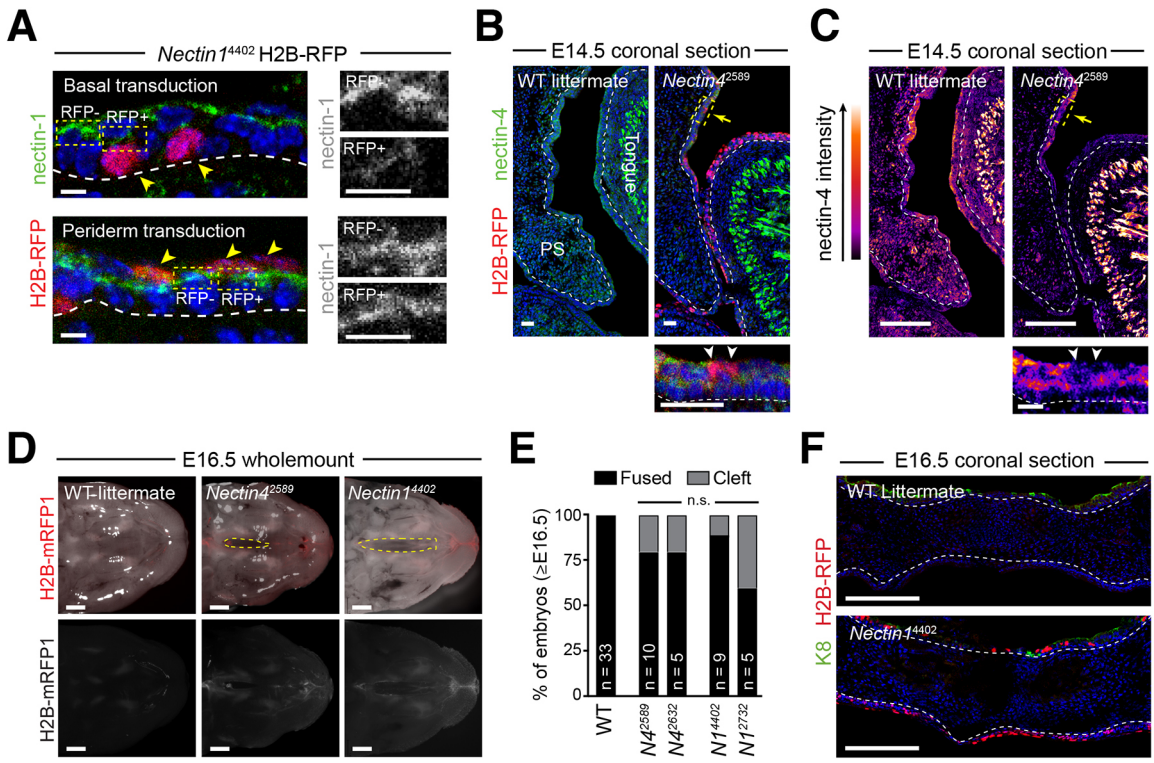

Fig. 2. Depletion of one *Nectin* homolog is insufficient to cause highly penetrant CP. (A) E14.5 *Nectin1*^{4402}-transduced palatal epithelia immunostained for nectin 1 (green) and H2B-RFP reporter (red). Boxed regions show nectin 1 in greyscale. (B,C) Immunofluorescent images (B) and LUT intensity plots (C) of E14.5 *Nectin4*^{2589} and wild-type PS showing loss of nectin 4 in H2B-RFP+ cells. Bottom panels are detailed views of the boxed regions (highlighted by yellow arrows) in the top panels. Arrowheads in the bottom panels indicate RFP^{+} periderm cells. (D) Dark-field (top) and fluorescent (bottom) stereoscope images of E16.5 wild-type (left), *Nectin4*^{2589} (middle) and *Nectin1*^{4402} (right) infected embryos, as in Fig. 1C. (E) Rate of CP penetrance in *Nectin1* and *Nectin4* knockdown embryos. (F) E16.5 palate in *Nectin1*^{4402} embryo showing complete fusion. Scale bars: 4 µm in A; 25 µm in B,C; 1 mm in D; 100 µm in F.

mutations, predicted to truncate the protein following the first Ig-like loop, maintaining the region that mediates *trans* heterodimerization while eliminating the transmembrane region and afadin binding (Lough et al., 2017; Suzuki et al., 2000; Yoshida et al., 2015). One of the better characterized CLPED1 disease variants is the *NECTIN1*^{W185X} nonsense mutation (Sozen et al., 2001; Suzuki et al., 2000). Although it is not known whether truncated *NECTIN1* transcripts undergo nonsense-mediated decay, it is conceivable that they could function in a dominant-negative manner by forming unproductive heterotypic interactions that interfere with other nectin binding. As evidence of this, an Fc-fusion of the first Ig-like loop of nectin 1 has been used to bind to and inhibit endogenous interactions between nectins 1, 3 and 4 (Kawakatsu et al., 2002). If this were the case, expression of the *NECTIN1*^{W185X} variant would be more detrimental than *Nectin1* loss.

To test this, we created a bicistronic lentiviral construct to express human *NECTIN1*^{W185X} with a C-terminal V5 epitope tag, together with an H2B-mRFP1 reporter. To mimic homozygosity of the *NECTIN1*^{W185X} mutation, we included the *Nectin1*^{4402} shRNA to knock down endogenous murine *Nectin1* (Fig. 4A). In E16.5 *Nectin1*^{4402}; *NECTIN1*^{W185X} palatal epithelium, both the reporter, labeling transduced cells and the V5 tag (which labels the truncated NECTIN^{W185X} protein) could be visualized (Fig. 4B). Although all *Nectin1*^{4402}; *NECTIN1*^{W185X} PS underwent normal elevation, most failed to approximate (4/7 embryos; 2 litters), whereas the other three displayed a persistent MES with abnormal epithelial organization (Fig. 4C,D). MES dissolution phenotypes have also been reported upon epithelial loss of *Tgfbr1/2* (Dudas et al., 2006; Xu et al., 2006) and *Myh9* (Kim et al., 2015). However, these mutants display a persistent, bilayered MES, while we observe a highly disorganized epithelium with islands of cells – many of which are RFP+ – within the mesenchyme. As these islands are E-cadherin+, we believe they are likely epithelial in origin, rather than lentiviral transduced mesenchymal cells. Because MES cells normally undergo coordinated displacement towards the oral and nasal epithelial surfaces (Kim et al., 2015), it is tempting to speculate that these residual epithelial islands result from errors in this coordinated migration, possibly owing to the known function of nectins in epithelial cell sorting (Katsunuma et al., 2016; Togashi et al., 2011).

Four lines of evidence support the conclusion that the truncated *NECTIN1*^{W185X} protein functions in a dominant-interfering manner. First, the penetrance of palate closure defects was much higher in *Nectin1*^{4402}; *NECTIN1*^{W185X} embryos compared with *Nectin1*^{4402} knockdowns (100% vs 11%). Second, *Nectin1*^{4402}; *NECTIN1*^{W185X} embryos display MES dissolution defects not observed in either *Nectin1* or *Nectin4* knockdowns. Third, the subcellular localization of *NECTIN1*^{W185X} is abnormal; it fails to accumulate at the basal cell-periderm interface – instead displaying circumferential, cytoplasmic accumulation (Fig. 4E). Furthermore, although the *Nectin1*^{4402} shRNA acts cell autonomously in basal cells, expression of *NECTIN1*^{W185X} in periderm was sufficient to disrupt endogenous nectin 1 localization non-cell autonomously in neighboring basal cells (Fig. 4F). Fourth, we observed syndactyly – a clinical feature of CLPED1 where digits are fused – in 2/7 *NECTIN1*^{W185X} mutant embryos, but never in *Nectin1* or *Nectin4* knockdowns (Fig. 4G). It should be noted, however, that we cannot exclude the possibility that the *NECTIN1*^{W185X} mutation confers gain-of-function activity, which could be tested by overexpression on a wild-type rather than *Nectin1* knockdown background.

The presence of intraoral adhesions and syndactyly in various nectin/afadin perturbations suggests the most likely mechanism of

Development (2020) 147, dev189241. doi:10.1242/dev.189241

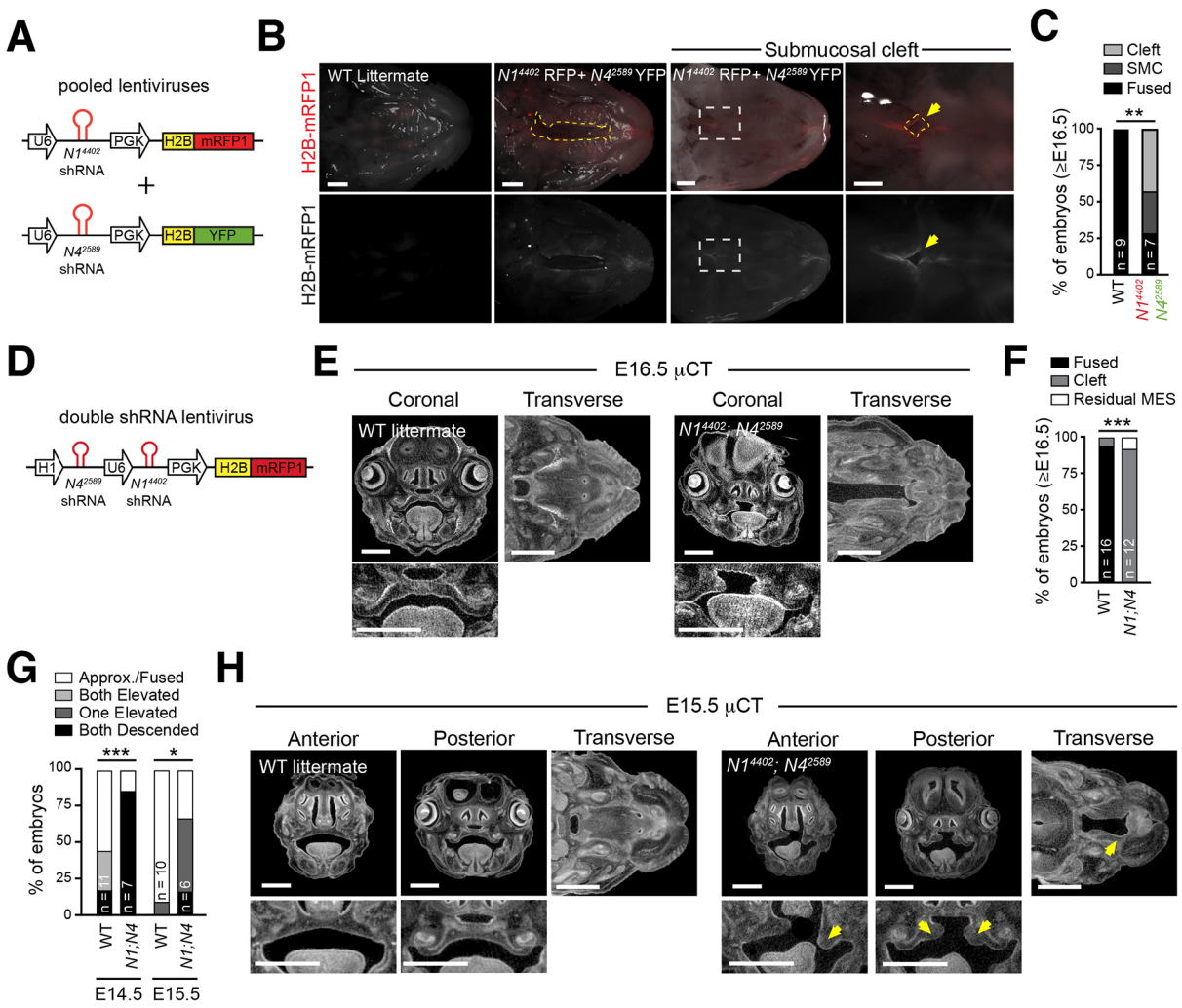

Fig. 3. *Nectin1* and *Nectin4* cooperate to promote palate closure. (A) Pooled lentiviral approach for dual *Nectin1/4* knockdown. (B) Dark-field (top) and fluorescent (bottom) stereoscope images of E16.5 *Nectin1*^{4402} H2B-RFP/*Nectin4*^{2589} H2B-YFP infected embryo, as in Fig. 1C. Boxed region shows submucosal cleft (SMC, yellow arrow). (C) Quantification of palatal phenotypes in *Nectin1*^{4402} H2B-RFP/*Nectin4*^{2589} H2B-YFP embryos. (D) Double shRNA lentiviral construct for simultaneous *Nectin1*/*Nectin4* knockdown. (E) Contrast-enhanced µCT images of E16.5 *Nectin1*^{4402}; *Nectin4*^{2589} and littermate heads. (F,G) Quantification of palate fusion phenotypes in wild-type and *Nectin1*^{4402}; *Nectin4*^{2589} embryos at indicated ages. (H) E15.5 µCT images of *Nectin1*^{4402}; *Nectin4*^{2589} and littermate heads; yellow arrows indicate unilateral partially descended PS. Scale bars: 1 mm in B,E,H. *P<0.05, **P<0.01,*** P<0.001 (Fisher's exact test).

action for the *NECTIN1*^{W185X} mutation is disrupting periderm formation or function. Interestingly, there are some parallels in how epithelial cells and periderm coordinate morphogenesis in both palatogenesis and digit separation. For example, during digit separation, epithelial cells form an interdigital epithelial tongue (IET) similar to the MES, with non-adhesive periderm cells functioning to prevent aberrant interdigital adhesions (Kashgari et al., 2020).

In conclusion, our study demonstrates the utility of LUGGIGE in creating allelic series, compound mutants and human disease variants for studying human genetic disorders such as CP. Our results also resolve longstanding uncertainty regarding the role of nectins in mammalian palatogenesis, confirming that, despite the lack of CP in *Nectin1* germline knockouts, the nectin-afadin axis is required for normal palate elevation and fusion.

MATERIALS AND METHODS

Animals

Mice were housed in an AAALAC-accredited (329; June 2017), USDA registered (55-R-0004), NIH welfare-assured [D16-00256 (A3410-01)] animal facility. All procedures were performed under IACUC-approved animal protocols (19-155). CD1 mice (Charles River; 022) were used for all shRNA experiments. *Afdn*$^{fl/fl}$ animals (Beaudoin et al., 2012) were maintained on a mixed C57B6/J CD1 background and either bred to the same *Krt14-Cre* allele (Dassule et al., 2000) or injected with lentiviral Cre-mRFP1 (see below). The procedure for producing, concentrating and injecting lentivirus into amniotic fluid of E9.5 embryos has been previously described (Beronja et al., 2010) and is briefly detailed below.

Lentiviral injections

This protocol is approved via IACUC #19-155. Pregnant CD1 or *Afdn*$^{fl/fl}$ females were anesthetized and the uterine horn pulled into a PBS filled dish to expose the E9.5 embryos. Embryos and custom-made glass needles were visualized by ultrasound (Vevo 2100) to guide microinjection of ∼0.7 µl of concentrated lentivirus into the amniotic space. Three to ten embryos were injected depending on litter size. Following injection, the uterine horn(s) were reinserted into the mother's abdominal cavity, which was sutured closed. The incision in the skin was resealed with surgical staples and the mother was provided with subcutaneous analgesics (5 mg/kg meloxicam and 1-4 mg/kg bupivacaine). Once awake and freely moving, the mother was returned to her housing facility for 4-9 days, at which point E13.5-18.5 embryos were harvested and processed accordingly.

Development (2020) 147, dev189241. doi:10.1242/dev.189241

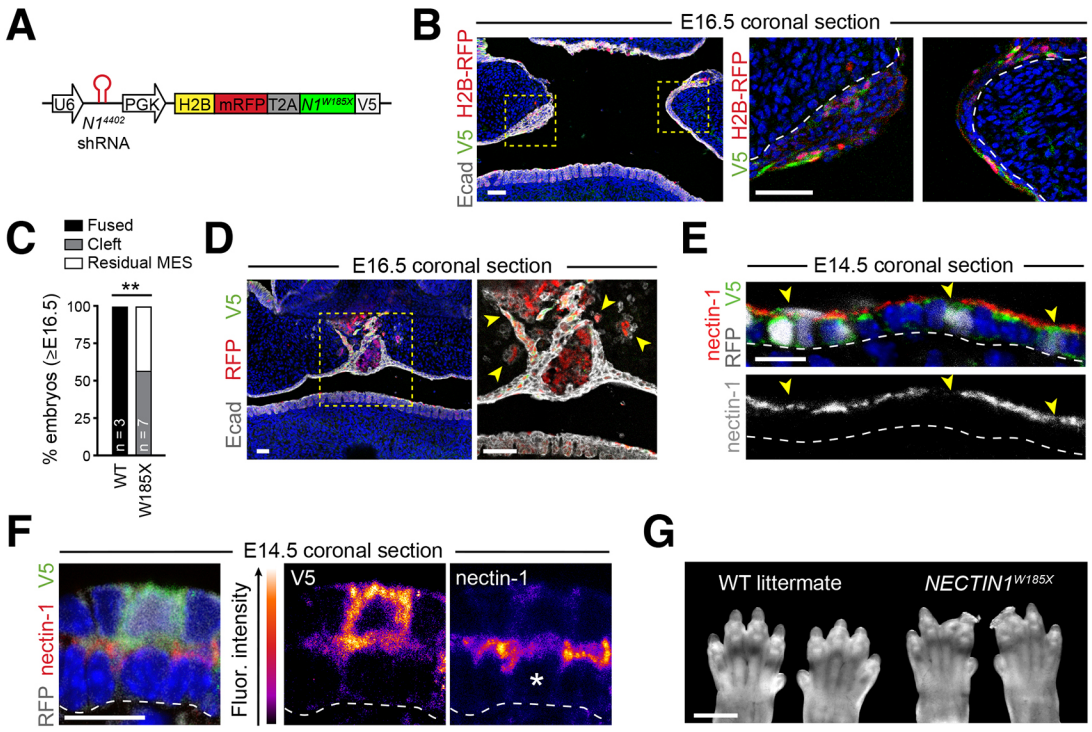

Fig. 4. CLPED1 variant W185X acts in a dominant interfering fashion to cause CP. (A) *NECTIN1*^{W185X} CLPED1 mutant lentiviral construct. (B) E16.5 *NECTIN1*^{W185X} oral cavity with CP, showing V5-tagged truncated nectin 1 (green) and H2B-RFP reporter (red) expression in E-cadherin+ epithelial cells (gray). Boxed regions are shown in more detail on the right. (C) Quantification of palatal phenotypes in *NECTIN1*^{W185X} mutant embryos. (D) E16.5 *NECTIN1*^{W185X} oral cavity showing disorganized residual MES, marked by E-cad+ (gray) epithelia within palatal mesenchyme. Boxed region is shown in more detail on the right; arrowheads label 'epithelial islands'. (E) E14.5 *NECTIN1*^{W185X} palatal epithelia showing V5-tagged *NECTIN1*^{W185X} transgene (green) together with endogenous nectin 1 (red); the nectin-1 antibody does not recognize the W185X variant. Arrowheads indicate H2B-RFP^{+} basal palatal epithelia. (F) Immunofluorescent and LUT intensity images showing non-cell autonomous reduction of endogenous nectin 1 in basal cell (*). (G) Dark-field stereoscope images of E16.5 *NECTIN1*^{W185X} forepaws, showing syndactyly of the first two digits. Scale bars: 50 µm in B,D; 10 µm in E,F; 1 mm in G. $^{**}P<0.01$ (Fisher's exact test).

Micro computerized tomography (µCT) imaging

E14.5-E16.5 embryos were decapitated and heads were fixed for 90 min in 4% paraformaldehyde at room temperature and rinsed with PBS. Heads were then submerged in a 0.3% (w/v) solution of phosphotungstic acid hydrate (Sigma-Aldrich P4006) and diluted in 70% ethanol for 72 h or longer with agitation. Samples were rinsed in PBS for >20 min prior to image collection using a Scanco Medical microCT-40 machine using a holder with diameter of 12 mm, voxel size of 6 µm and 114 µA/70 kVp/8 W energy exposure.

Constructs and RNAi

For *Nectin1* and *Nectin4* RNAi targeting, we tested ∼10 shRNAs for knockdown efficiency in primary keratinocytes. These sequences were selected from The RNAi Consortium (TRC) Mission shRNA library (Sigma) versions 1.0, 1.5 and 2.0, and cloned using complementary annealed oligonucleotides with AgeI/EcoRI linkers. For *Afdn*, we used an shRNA that had been previously validated with our lentiviral injection technique (Lough et al., 2019). shRNA clones are identified by the gene name with the nucleotide base (NCBI Accession number) where the 21-nucleotide target sequence begins in superscript (e.g. *Afdn*^{2711}). Lentivirus was packaged in 293FT or TN cells using the pMD2.G and psPAX2 helper plasmids (Addgene plasmids 12259 and 12260, respectively). For knockdown screening, primary keratinocytes were seeded at a density of ∼150,000 cells per well into six-well plates and grown to ∼80% confluency in E-Low calcium medium and infected with an MOI of ∼1. Approximately 48 h post-infection, keratinocytes were treated with puromycin (2 µg/ml) to generate stable cell lines. After 3-4 days of puromycin selection, cells were lysed and RNA isolated using the RNeasy Mini Kit (Qiagen). cDNA was generated and amplified from 10-200 µg total RNA using either Superscript VILO (Invitrogen) or iScript (Bio-Rad). mRNA knockdown was determined by RT-qPCR (Applied Biosystems 7500 Fast RT-PCR) using two independent primer sets for each transcript with *Hprt1* and cyclophilin B (*Ppib2*) as reference genes and cDNA from stable cell lines expressing *Scramble* shRNA as a reference control. Knockdown efficiencies (±95% confidence interval) were as follows: *Nectin1*^{4402} (56.2±8.2%), *Nectin1*^{2732} (53.6±12.8%), *Nectin4*^{2589} (82.5±32.9%) and *Nectin4*^{2632} (52.5±8.0%). Primer efficiencies were determined using dose-response curves and were required to be greater than 1.8, with relative transcript abundance determined by the ΔΔCT method. RT-qPCR runs were performed in triplicate with the mean knockdown efficiency determined by calculating the geometric mean of the ΔΔCT values for at least two independent technical replicates. The following primer sequences were used: *Nectin4* (fwd-1, 5′-CAGCCCCCTCCCAAATACAA-3′; rev-1, 5′-TATGATCACTGAGGCGGACACC-3′; fwd-2, 5′-AGATGTGGGGCCCTGAAGC-3′; rev-2, 5′-GCATTCGTACTCGCCCTCATC-3′) and *Nectin1* (fwd-1, 5′-TAACCCGCCAGCCACTGAGT-3′; rev-1, 5′-CTGCGCAGGGCCACTATGA-3′; fwd-2, 5′-CAAACAGAACATGGCCATCTACAAC-3′; rev-2, 5′-TCGCCCTTTAGCCGTGTTTC-3′). The following shRNA targeting sequences were used: *Afdn*^{2711} (5′-CCTGATGACATTCCAAATATA-3′), *Nectin1*^{4402} (5′-TAAACGAGAAACCTGTATTAA-3′), *Nectin1*^{2732} (5′-GAATGCGAGGCACAGAATTAT-3′), *Nectin4*^{2589} (5′-TACGTACCTTCTGTAAATTAA-3′) and *Nectin4*^{2631} (5′-CTGCTTAGACTCCCTTAATAA-3′).

Antibodies, immunohistochemistry, and fixed imaging

E13.5-16.5 embryonic heads were fixed for 1 h at room temperature in 4% paraformaldehyde (in PBS) and submerged in 15% sucrose overnight (4°C). The next day, heads were submerged in 30% sucrose at room temperature for >6 h (until they sank) then mounted whole in OCT (Tissue Tek) and frozen at −20°C. Infected and uninfected littermate controls were mounted in the same blocks to allow for direct comparisons on the same slide. Frozen samples were sectioned (8-12 µm thick) on a Leica CM1950 cryostat, mounted on SuperFrost Plus slides (ThermoFisher) and stored at −80°C. For staining, sections were thawed at 37°C for 15 min, washed with PBS and

Development (2020) 147, dev189241. doi:10.1242/dev.189241

blocked for 1 h with gelatin block (5% NDS, 3% BSA, 8% cold-water fish gelatin, 0.05% Triton X-100 in PBS). Primary antibodies were diluted in gelatin block and incubated overnight in a humidity chamber at 4°C. Slides were then washed with PBS and incubated with secondary antibodies diluted in gelatin block at room temperature (~25°C) for 2 h, counterstained with DAPI (1:2000) for 5 min and mounted in ProLong Gold (Invitrogen). Images were acquired using LAS AF software on a Leica TCS SPE-II 4 laser confocal system on a DM5500 microscope with an ACS Apochromat 20×/0.60 multi-immersion, an ACS Apochromat 40×/1.15 oil-immersion or an ACS Apochromat 63×/1.30 oil-immersion objective.

The following primary antibodies were used: anti-mCherry (rat, Life Technologies M11217, 1:1000-3000), anti-GFP (chicken, Abcam ab13970, 1:1000), anti-E-cadherin (rat, Life Technologies 131900, 1:1000), anti-E-cadherin (goat, R&D Systems AF748, 1:1000), anti-afadin (rabbit, Sigma A0224, 1:500), anti-nectin 1 (rat, MBL International D146-3, 1:250), anti-nectin 4 (rabbit, Millipore HPA010775, 1:100), anti-K14 (guinea pig, OriGene BP5009, 1:1000), anti-K8 (rat, Developmental Studies Hybridoma Bank TROMA-1, 1:500) and anti-V5 (rabbit, Abcam ab9113, 1:500).

The following secondary antibodies were used (all antibodies were highly cross-absorbed and produced in donkey): anti-rabbit AlexaFluor 488 (Life Technologies, 1:1000), anti-rabbit Rhodamine Red-X (Jackson Labs, 1:500), anti-rabbit Cy5 (Jackson Labs, 1:400), anti-rat AlexaFluor 488 (Life Technologies, 1:1000), anti-rat Rhodamine Red-X (Jackson Labs, 1:500), anti-rat Cy5 (Jackson Labs, 1:400), anti-guinea pig AlexaFluor 488 (Life Technologies, 1:1000), anti-guinea pig Rhodamine Red-X (Jackson Labs, 1:500), anti-guinea pig Cy5 (Jackson Labs, 1:400), anti-goat AlexaFluor 488 (Life Technologies, 1:1000) and anti-goat Cy5 (Jackson Labs, 1:400).

Keratinocyte culture and calcium-shift assays

Primary mouse keratinocytes were maintained in E medium with 15% chelated FBS and 50 µM $CaCl_2$ (E low medium). Parental cell lines tested negative for mycoplasma infection using the ATCC 30-1012 K kit. For viral infection, keratinocytes were plated at ~150,000 cells per well in a six-well plate, incubated with lentivirus in the presence of polybrene (1 µg/ml) and centrifuged at 1100 ***g*** for 30 min at 37°C. Stable cell lines were generated/maintained by adding puromycin (2 µg/ml) 48 h after infection and continual antibiotic treatment following. Calcium shifts were performed by seeding ~45,000 cells per well into 8-well Permanox chamber slides (Lab-Tek 177445) coated with poly-L-lysine, collagen and fibronectin. Once cells reached ~85% confluency (~12-16 h) cells were switched to high Ca^{2+} (1.5 mM) medium and grown for 8 h. Cells were fixed with 4% paraformaldehyde in PBS warmed to room temperature. Immunostaining was performed using the same protocol as for slides (see above).

Measurements, quantification, graphing and statistics

Palatogenesis phenotypes, including CP, residual MES, submucosal cleft and the orientation of the PS, were determined by either stereoscopic imaging (as in Fig. 1C), µCT scanning (as in Fig. 1E), or cryosectioning and immunofluorescent confocal imaging (as in Fig. 1H). For animals E16.5 or older, statistical testing between genotypes was performed using Fisher's exact test, with a binary grouping of phenotypes into either 'fused' or 'abnormal' groups, the latter of which included embryos displaying submucosal cleft or residual MES, as well as classic CP. For younger timepoints (i.e. E14.5 or E15.5) statistical testing was performed by binning the number of PS that were elevated or descended in each genotype (i.e. for Fig. 1G, wild-type E15.5 animals had 30 PS elevated and 0 descended, while *Afdn*^{2711} animals had four PS elevated and four descended) and evaluating significance using Fisher's exact test. All statistical analyses and graphs were generated using GraphPad Prism 8. Figures were assembled using Adobe Photoshop and Illustrator CC 2020.

Acknowledgements

We thank members of the Williams Lab for their critical feedback throughout the process. We thank Dr Louis Reichardt (UCSF) and Dr Gerard M. Beaudoin III (Trinity University) for sharing the *Afdn*$^{fl/fl}$ strain. We thank Dr. Hong Yuan, Jon Frank and the Small Animal Imaging Facility at the UNC Biomedical Imaging Research Center for providing the µCT imaging service. The imaging core is supported in part by an NCI cancer core grant (P30-CA016086-40).

Competing interests

The authors declare no competing or financial interests.

Author contributions

Conceptualization: K.J.L., K.M.B., S.E.W.; Methodology: K.J.L., K.M.B.; Validation: K.J.L.; Formal analysis: K.J.L., S.E.W.; Investigation: K.J.L., D.C.S., A.J.B., J.J.W.; Resources: S.E.W.; Writing - original draft: K.J.L.; Writing - review & editing: K.J.L., D.C.S., A.J.B., J.J.W., K.M.B., S.E.W.; Visualization: K.J.L.; Supervision: K.J.L., S.E.W.; Project administration: K.J.L., S.E.W.; Funding acquisition: K.J.L., S.E.W.

Funding

K.J.L. was supported by a National Institutes of Health Ruth L. Kirschstein Predoctoral National Research Service Award (F31 DE026956). K.M.B. was supported by a National Institutes of Health/National Institute of Dental and Craniofacial Research K08 Mentored Clinical Scientist Research Career Development Award (DE026537) and by L40 (Loan Repayment Program for Pediatric Researcher). S.W. was supported by a Sidney Kimmel Foundation for Cancer Research Scholar Award (SKF-15-165). Deposited in PMC for release after 12 months.

Supplementary information

Supplementary information available online at
https://dev.biologists.org/lookup/doi/10.1242/dev.189241.supplemental

Peer review history

The peer review history is available online at
https://dev.biologists.org/lookup/doi/10.1242/dev.189241.reviewer-comments.pdf

References

Andl, T., Ahn, K., Kairo, A., Chu, E. Y., Wine-Lee, L., Reddy, S. T., Croft, N. J., Cebra-Thomas, J. A., Metzger, D., Chambon, P. et al. (2004). Epithelial Bmpr1a regulates differentiation and proliferation in postnatal hair follicles and is essential for tooth development. *Development* **131**, 2257-2268. doi:10.1242/dev.01125

Barron, M. J., Brookes, S. J., Draper, C. E., Garrod, D., Kirkham, J., Shore, R. C. and Dixon, M. J. (2008). The cell adhesion molecule nectin-1 is critical for normal enamel formation in mice. *Hum. Mol. Genet.* **17**, 3509-3520. doi:10.1093/hmg/ddn243

Beaudoin, 3rd, G. M., Schofield, C. M., Nuwal, T., Zang, K., Ullian, E. M., Huang, B. and Reichardt, L. F. (2012). Afadin, a Ras/Rap effector that controls cadherin function, promotes spine and excitatory synapse density in the hippocampus. *J. Neurosci.* **32**, 99-110. doi:10.1523/JNEUROSCI.4565-11.2012

Beronja, S., Livshits, G., Williams, S. and Fuchs, E. (2010). Rapid functional dissection of genetic networks via tissue-specific transduction and RNAi in mouse embryos. *Nat. Med.* **16**, 821-827. doi:10.1038/nm.2167

Bouchard, M. J., Dong, Y., McDermott, Jr., B. M., Lam, D.-H., Brown, K. R., Shelanski, M., Bellve, A. R. and Racaniello, V. R. (2000). Defects in nuclear and cytoskeletal morphology and mitochondrial localization in spermatozoa of mice lacking nectin-2, a component of cell-cell adherens junctions. *Mol. Cell. Biol.* **20**, 2865-2873. doi:10.1128/MCB.20.8.2865-2873.2000

Brancati, F., Fortugno, P., Bottillo, I., Lopez, M., Josselin, E., Boudghene-Stambouli, O., Agolini, E., Bernardini, L., Bellacchio, E., Iannicelli, M. et al. (2010). Mutations in PVRL4, encoding cell adhesion molecule nectin-4, cause ectodermal dysplasia-syndactyly syndrome. *Am. J. Hum. Genet.* **87**, 265-273. doi:10.1016/j.ajhg.2010.07.003

Bush, J. O. and Jiang, R. (2012). Palatogenesis: morphogenetic and molecular mechanisms of secondary palate development. *Development* **139**, 231-243. doi:10.1242/dev.067082

Bustos, T., Simosa, V., Pinto-Cisternas, J., Abramovits, W., Jolay, L., Rodriguez, L., Fernandez, L. and Ramela, M. (1991). Autosomal recessive ectodermal dysplasia: I. An undescribed dysplasia/malformation syndrome. *Am. J. Med. Genet.* **41**, 398-404. doi:10.1002/ajmg.1320410403

Byrd, K. M., Lough, K. J., Patel, J. H., Descovich, C. P., Curtis, T. A. and Williams, S. E. (2016). LGN plays distinct roles in oral epithelial stratification, filiform papilla morphogenesis and hair follicle development. *Development* **143**, 2803-2817. doi:10.1242/dev.136010

Dassule, H. R., Lewis, P., Bei, M., Maas, R. and McMahon, A. P. (2000). Sonic hedgehog regulates growth and morphogenesis of the tooth. *Development* **127**, 4775-4785.

Dixon, M. J., Marazita, M. L., Beaty, T. H. and Murray, J. C. (2011). Cleft lip and palate: understanding genetic and environmental influences. *Nat. Rev. Genet.* **12**, 167-178. doi:10.1038/nrg2933

Dudas, M., Kim, J., Li, W. Y., Nagy, A., Larsson, J., Karlsson, S., Chai, Y. and Kaartinen, V. (2006). Epithelial and ectomesenchymal role of the type I TGF-beta receptor ALK5 during facial morphogenesis and palatal fusion. *Dev. Biol.* **296**, 298-314. doi:10.1016/j.ydbio.2006.05.030

El-Brolosy, M. A., Kontarakis, Z., Rossi, A., Kuenne, C., Günther, S., Fukuda, N., Kikhi, K., Boezio, G. L. M., Takacs, C. M., Lai, S. L. et al. (2019). Genetic

compensation triggered by mutant mRNA degradation. *Nature* **568**, 193-197. doi:10.1038/s41586-019-1064-z

Ferone, G., Thomason, H. A., Antonini, D., De Rosa, L., Hu, B., Gemei, M., Zhou, H., Ambrosio, R., Rice, D. P., Acampora, D. et al. (2012). Mutant p63 causes defective expansion of ectodermal progenitor cells and impaired FGF signalling in AEC syndrome. *EMBO Mol. Med.* **4**, 192-205. doi:10.1002/emmm.201100199

Greene, R. M. and Pratt, R. M. (1976). Developmental aspects of secondary palate formation. *J. Embryol. Exp. Morphol.* **36**, 225-245.

Hammond, N. L., Dixon, J. and Dixon, M. J. (2019). Periderm: Life-cycle and function during orofacial and epidermal development. *Semin. Cell Dev. Biol.* **91**, 75-83. doi:10.1016/j.semcdb.2017.08.021

Ikeda, W., Nakanishi, H., Miyoshi, J., Mandai, K., Ishizaki, H., Tanaka, M., Togawa, A., Takahashi, K., Nishioka, H., Yoshida, H. et al. (1999). Afadin: A key molecule essential for structural organization of cell-cell junctions of polarized epithelia during embryogenesis. *J. Cell Biol.* **146**, 1117-1132. doi:10.1083/jcb.146.5.1117

Inagaki, M., Irie, K., Ishizaki, H., Tanaka-Okamoto, M., Morimoto, K., Inoue, E., Ohtsuka, T., Miyoshi, J. and Takai, Y. (2005). Roles of cell-adhesion molecules nectin 1 and nectin 3 in ciliary body development. *Development* **132**, 1525-1537. doi:10.1242/dev.01697

Kashgari, G., Meinecke, L., Gordon, W., Ruiz, B., Yang, J., Ma, A. L., Xie, Y., Ho, H., Plikus, M. V., Nie, Q. et al. (2020). Epithelial Migration and Non-adhesive Periderm Are Required for Digit Separation during Mammalian Development. *Dev. Cell* **52**, 764-778e764. doi:10.1016/j.devcel.2020.01.032

Katsunuma, S., Honda, H., Shinoda, T., Ishimoto, Y., Miyata, T., Kiyonari, H., Abe, T., Nibu, K., Takai, Y. and Togashi, H. (2016). Synergistic action of nectins and cadherins generates the mosaic cellular pattern of the olfactory epithelium. *J. Cell Biol.* **212**, 561-575. doi:10.1083/jcb.201509020

Kawakatsu, T., Shimizu, K., Honda, T., Fukuhara, T., Hoshino, T. and Takai, Y. (2002). Trans-interactions of nectins induce formation of filopodia and Lamellipodia through the respective activation of Cdc42 and Rac small G proteins. *J. Biol. Chem.* **277**, 50749-50755. doi:10.1074/jbc.M209846200

Kim, S., Lewis, A. E., Singh, V., Ma, X., Adelstein, R. and Bush, J. O. (2015). Convergence and extrusion are required for normal fusion of the mammalian secondary palate. *PLoS Biol.* **13**, e1002122. doi:10.1371/journal.pbio.1002122

Kousa, Y. A., Mansour, T. A., Seada, H., Matoo, S. and Schutte, B. C. (2017). Shared molecular networks in orofacial and neural tube development. *Birth Defects Res.* **109**, 169-179. doi:10.1002/bdra.23598

Li, H., Jones, K. L., Hooper, J. E. and Williams, T. (2019). The molecular anatomy of mammalian upper lip and primary palate fusion at single cell resolution. *Development* **146**. https://dev.biologists.org/content/146/12/dev174888

Lough, K. J., Byrd, K. M., Spitzer, D. C. and Williams, S. E. (2017). Closing the Gap: Mouse Models to Study Adhesion in Secondary Palatogenesis. *J. Dent. Res.* **96**, 1210-1220. doi:10.1177/0022034517726284

Lough, K. J., Byrd, K. M., Descovich, C. P., Spitzer, D. C., Bergman, A. J., Beaudoin, G. M., Reichardt, L. F. and Williams, S. E. (2019). Telophase correction refines division orientation in stratified epithelia. *eLife* **8**. https://elifesciences.org/articles/49249

Mandai, K., Nakanishi, H., Satoh, A., Obaishi, H., Wada, M., Nishioka, H., Itoh, M., Mizoguchi, A., Aoki, T., Fujimoto, T. et al. (1997). Afadin: A novel actin filament-binding protein with one PDZ domain localized at cadherin-based cell-to-cell adherens junction. *J. Cell Biol.* **139**, 517-528. doi:10.1083/jcb.139.2.517

Miyahara, M., Nakanishi, H., Takahashi, K., Satoh-Horikawa, K., Tachibana, K. and Takai, Y. (2000). Interaction of nectin with afadin is necessary for its clustering at cell-cell contact sites but not for its cis dimerization or trans interaction. *J. Biol. Chem.* **275**, 613-618. doi:10.1074/jbc.275.1.613

Mollo, M. R., Antonini, D., Mitchell, K., Fortugno, P., Costanzo, A., Dixon, J., Brancati, F. and Missero, C. (2015). p63-dependent and independent mechanisms of nectin-1 and nectin-4 regulation in the epidermis. *Exp. Dermatol.* **24**, 114-119. doi:10.1111/exd.12593

Momose, Y., Honda, T., Inagaki, M., Shimizu, K., Irie, K., Nakanishi, H. and Takai, Y. (2002). Role of the second immunoglobulin-like loop of nectin in cell-cell adhesion. *Biochem. Biophys. Res. Commun.* **293**, 45-49. doi:10.1016/S0006-291X(02)00183-3

Mossey, P. A., Little, J., Munger, R. G., Dixon, M. J. and Shaw, W. C. (2009). Cleft lip and palate. *Lancet* **374**, 1773-1785. doi:10.1016/S0140-6736(09)60695-4

Reymond, N., Fabre, S., Lecocq, E., Adelaï¨de, J., Dubreuil, P. and Lopez, M. (2001). Nectin4/PRR4, a new afadin-associated member of the nectin family that trans-interacts with nectin1/PRR1 through V domain interaction. *J. Biol. Chem.* **276**, 43205-43215. doi:10.1074/jbc.M103810200

Richardson, R. J., Dixon, J., Jiang, R. and Dixon, M. J. (2009). Integration of IRF6 and Jagged2 signalling is essential for controlling palatal adhesion and fusion competence. *Hum. Mol. Genet.* **18**, 2632-2642. doi:10.1093/hmg/ddp201

Richardson, R., Mitchell, K., Hammond, N. L., Mollo, M. R., Kouwenhoven, E. N., Wyatt, N. D., Donaldson, I. J., Zeef, L., Burgis, T., Blance, R. et al. (2017). p63 exerts spatio-temporal control of palatal epithelial cell fate to prevent cleft palate. *PLoS Genet.* **13**, e1006828. doi:10.1371/journal.pgen.1006828

Rodini, E. S. and Richieri-Costa, A. (1990). Autosomal recessive ectodermal dysplasia, cleft lip/palate, mental retardation, and syndactyly: the Zlotogora-Ogur syndrome. *Am. J. Med. Genet.* **36**, 473-476. doi:10.1002/ajmg.1320360420

Sözen, M. A., Suzuki, K., Tolarova, M. M., Bustos, T., Fernández Iglesias, J. E. and Spritz, R. A. (2001). Mutation of PVRL1 is associated with sporadic, non-syndromic cleft lip/palate in northern Venezuela. *Nat. Genet.* **29**, 141-142. doi:10.1038/ng740

Suzuki, K., Hu, D., Bustos, T., Zlotogora, J., Richieri-Costa, A., Helms, J. A. and Spritz, R. A. (2000). Mutations of PVRL1, encoding a cell-cell adhesion molecule/herpesvirus receptor, in cleft lip/palate-ectodermal dysplasia. *Nat. Genet.* **25**, 427-430. doi:10.1038/78119

Takahashi, K., Nakanishi, H., Miyahara, M., Mandai, K., Satoh, K., Satoh, A., Nishioka, H., Aoki, J., Nomoto, A., Mizoguchi, A. et al. (1999). Nectin/PRR: an immunoglobulin-like cell adhesion molecule recruited to cadherin-based adherens junctions through interaction with Afadin, a PDZ domain-containing protein. *J. Cell Biol.* **145**, 539-549. doi:10.1083/jcb.145.3.539

Togashi, H., Kominami, K., Waseda, M., Komura, H., Miyoshi, J., Takeichi, M. and Takai, Y. (2011). Nectins establish a checkerboard-like cellular pattern in the auditory epithelium. *Science* **333**, 1144-1147. doi:10.1126/science.1208467

Vasioukhin, V., Degenstein, L., Wise, B. and Fuchs, E. (1999). The magical touch: genome targeting in epidermal stem cells induced by tamoxifen application to mouse skin. *Proc. Natl Acad. Sci. USA* **96**, 8551-8556. doi:10.1073/pnas.96.15.8551

Walker, B. E. and Fraser, F. C. (1956). Closure of the Secondary Palate in Three Strains of Mice. *Development* **4**, 176-189.

Wu, C., Endo, M., Yang, B. H., Radecki, M. A., Davis, P. F., Zoltick, P. W., Spivak, R. M., Flake, A. W., Kirschner, R. E. and Nah, H. D. (2013). Intra-amniotic transient transduction of the periderm with a viral vector encoding TGFbeta3 prevents cleft palate in Tgfβ3−/− mouse embryos. *Mol. Ther.* **21**, 8-17. doi:10.1038/mt.2012.135

Xu, X., Han, J., Ito, Y., Bringas, Jr., P., Urata, M. M. and Chai, Y. (2006). Cell autonomous requirement for Tgfbr2 in the disappearance of medial edge epithelium during palatal fusion. *Dev. Biol.* **297**, 238-248. doi:10.1016/j.ydbio.2006.05.014

Yasumi, M., Shimizu, K., Honda, T., Takeuchi, M. and Takai, Y. (2003). Role of each immunoglobulin-like loop of nectin for its cell-cell adhesion activity. *Biochem. Biophys. Res. Commun.* **302**, 61-66. doi:10.1016/S0006-291X(03)00106-2

Yoshida, T., Miyoshi, J., Takai, Y. and Thesleff, I. (2010). Cooperation of nectin-1 and nectin-3 is required for normal ameloblast function and crown shape development in mouse teeth. *Dev. Dyn.* **239**, 2558-2569. doi:10.1002/dvdy.22395

Yoshida, M., Shimono, Y., Togashi, H., Matsuzaki, K., Miyoshi, J., Mizoguchi, A., Komori, T. and Takai, Y. (2012). Periderm cells covering palatal shelves have tight junctions and their desquamation reduces the polarity of palatal shelf epithelial cells in palatogenesis. *Genes Cells* **17**, 455-472. doi:10.1111/j.1365-2443.2012.01601.x

Yoshida, K., Hayashi, R., Fujita, H., Kubota, M., Kondo, M., Shimomura, Y. and Niizeki, H. (2015). Novel homozygous mutation, c.400C>T (p.Arg134*), in the PVRL1 gene underlies cleft lip/palate-ectodermal dysplasia syndrome in an Asian patient. *J. Dermatol.* **42**, 715-719. doi:10.1111/1346-8138.12882

Zhadanov, A. B., Provance, Jr., D. W., Speer, C. A., Coffin, J. D., Goss, D., Blixt, J. A., Reichert, C. M. and Mercer, J. A. (1999). Absence of the tight junctional protein AF-6 disrupts epithelial cell-cell junctions and cell polarity during mouse development. *Curr. Biol.* **9**, 880-888. doi:10.1016/S0960-9822(99)80392-3

Zlotogora, J. (1994). Syndactyly, ectodermal dysplasia, and cleft lip/palate. *J. Med. Genet.* **31**, 957-959. doi:10.1136/jmg.31.12.957

Zlotogora, J. and Ogur, G. (1988). Syndactyly, ectodermal dysplasia, and cleft lip and palate. *J. Med. Genet.* **25**, 503. doi:10.1136/jmg.25.7.503

Supplementary Figure 1

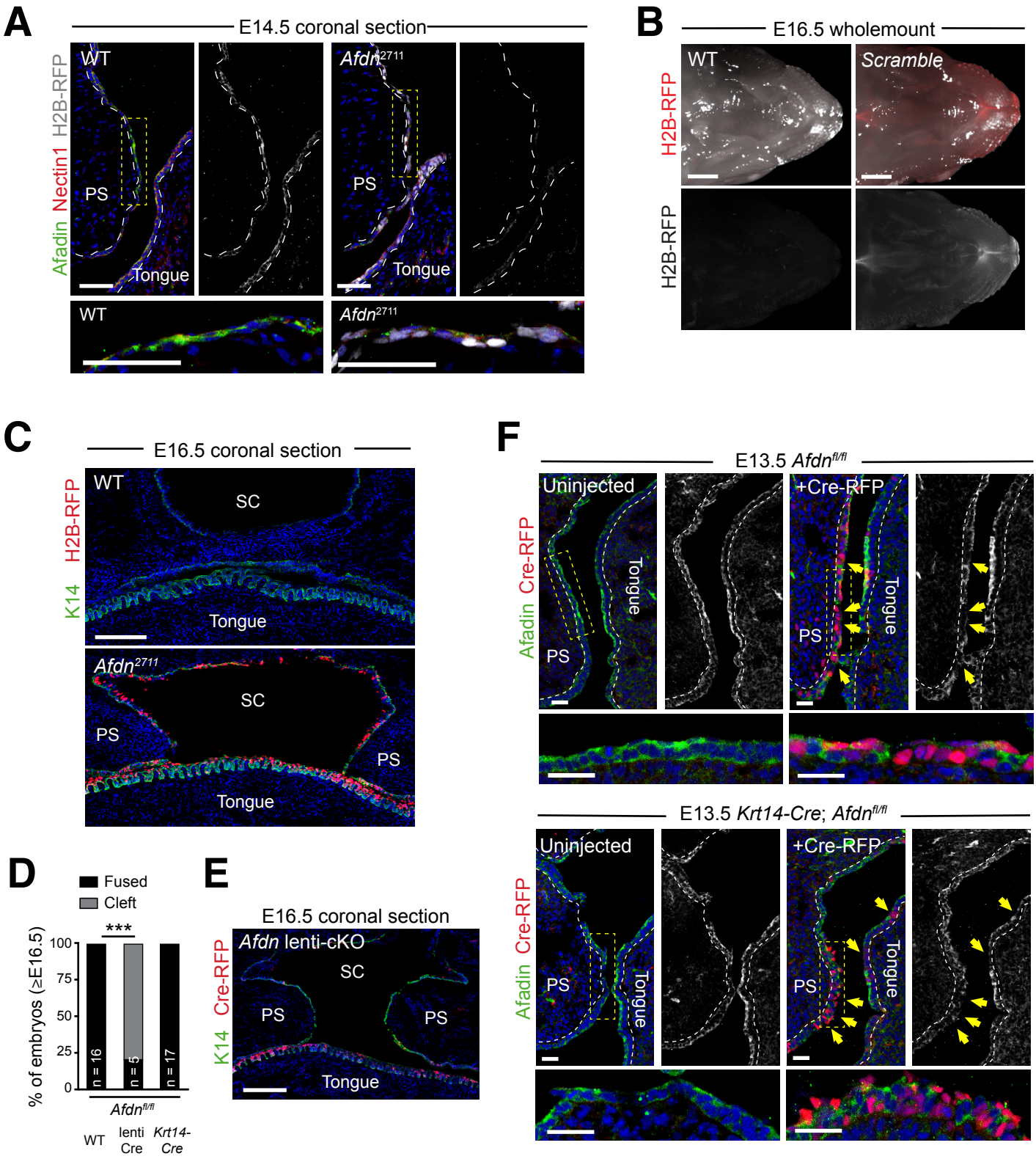

Figure S1 | Validation of transgenic models highlights improved efficacy of LUGGIGE

(A) E14.5 coronal sections of WT (left) and *Afdn*^{2711} (right) PS immunostained with Afadin (green), nectin-1 (red) and H2B-RFP (grey), demonstrating effective loss of Afadin accumulation in transduced epithelia; high magnification images of boxed region are shown in grayscale below. (B) Darkfield (top) and fluorescent (bottom) stereoscope images of E16.5 *Scramble H2B-RFP* infected embryo and uninjected littermate. H2B-RFP (red) is overlaid in the top panel. (C) Immunofluorescent image of E16.5 *Afdn*^{2711} and WT oral cavity. Some *Afdn*^{2711} embryos display normal PS elevation but fail to approximate. (D) Rate of CP phenotypes at E16.5 in *Afdn*$^{fl/fl}$ controls, *Afdn*$^{fl/fl}$ lenti-Cre, and *Afdn*$^{fl/fl}$ K14-Cre knockout littermates. *Afdn* knockout via lenti-Cre is suffient to cause CP, while K14-Cre is insufficient. (E) Immunofluorescent image of E16.5 *Afdn*$^{fl/fl}$ lenti-Cre oral cavity, demonstrating CP. (F) (Top) E13.5 *Afdn*$^{fl/fl}$ PS including Cre-RFP injected (right) and uninjected (left) samples stained for Afadin (green; grey isolated channel) and Cre-RFP (red). LUGGIGE-mediated recombination results in efficient loss of Afadin accumulation by E13.5. (Bottom) E13.5 *Krt14-Cre; Afdn*$^{fl/fl}$ PS including Cre-RFP injected (right) and uninjected (left) samples stained for Afadin (green; grey isolated channel) and Cre-RFP (red). While *Krt14-Cre; Afdn*$^{fl/fl}$ embryos still display robust Afadin signal (compared to uninjected *Afdn*$^{fl/fl}$ PS in Fig. S1C), addition of Cre-RFP results in mosaic loss of Afadin accumulation in transduced epithelia. High magnification images of boxed regions are shown below. Scale bars 50 μm (A), 1 mm (B), 200 μm (C,E), 25 μm (F). *** $P <$ 0.001, by Fisher's exact test.

Supplementary Figure 2

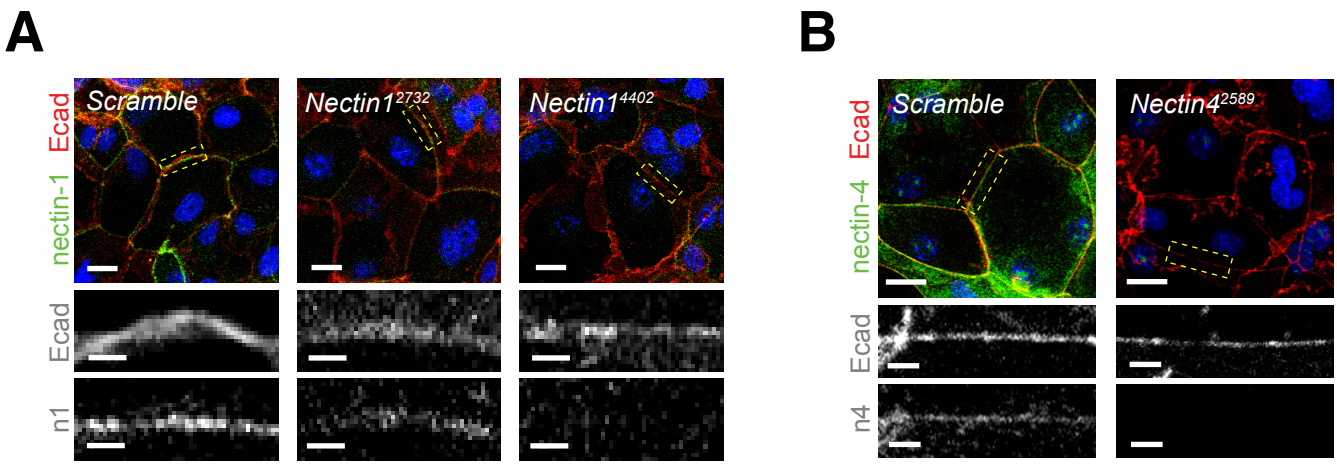

Figure S2 | *In vitro* validation of Nectin1/4 shRNA efficacy using calcium-shift assays

(A) Primary mouse keratinocytes after 8h Ca^{2+} shift—labeled with E-cad (red) and nectin-1 (green)—which accumulate in linear bands at cell-cell junctions. Yellow boxed region shown at high magnification below. *Nectin1*$_{4402}$ knockdown cells show robust loss of nectin-1, while *Nectin1*$_{2732}$ cells show intermediate loss compared to *Scramble* controls. (B) 8h Ca^{2+}-shifted keratinocytes stained for nectin-4 (green) and E-cad (red). *Nectin4*$_{2589}$ knockdown cells show robust loss of nectin-4 protein at cell-cell junctions. Scale bars 20 μm (large), 5 μm (zoom).

Supplementary Figure 3

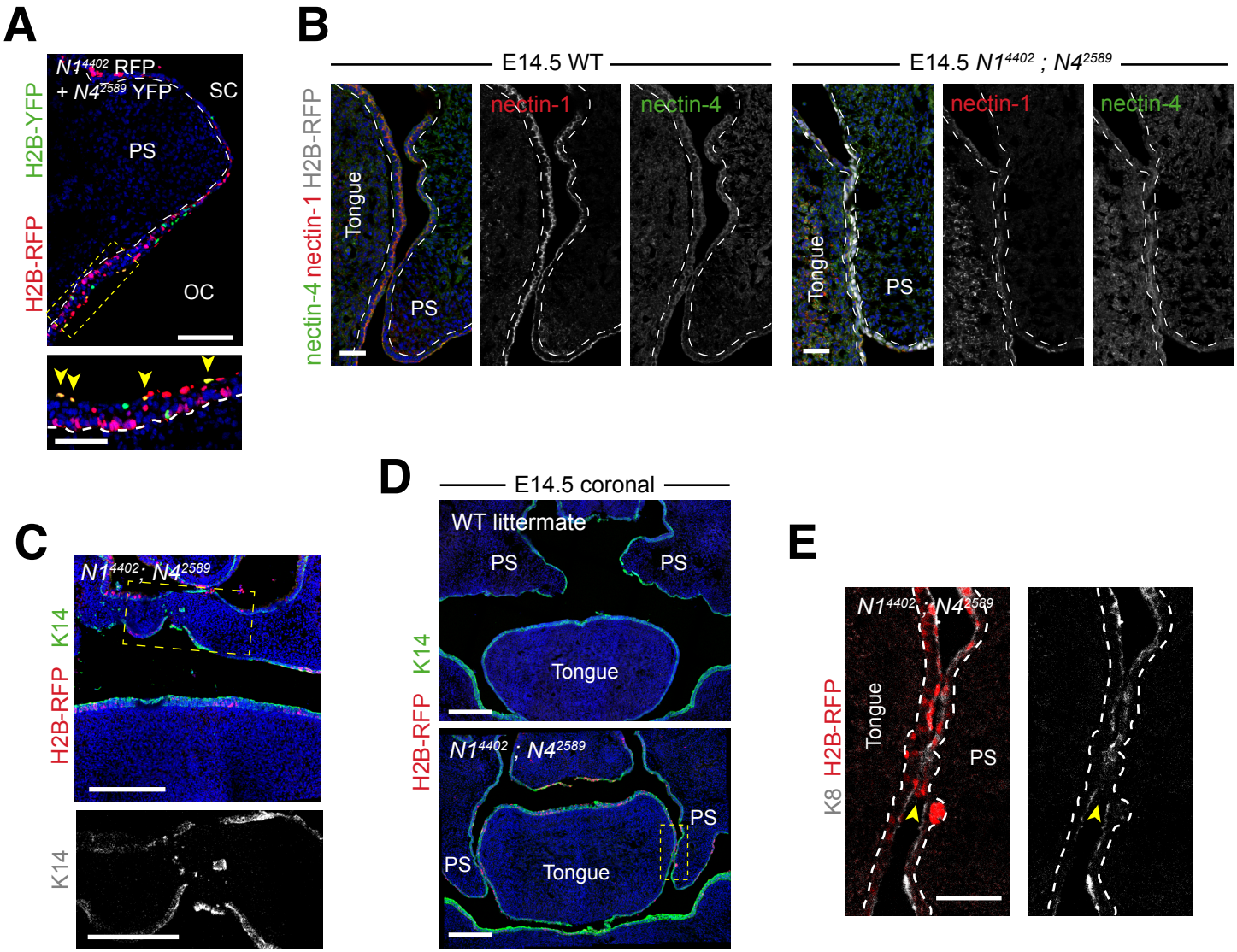

Figure S3 | Dual loss of *Nectin1* and *Nectin4* in a novel, double shRNA construct delays PS elevation and can result in residual MES.

(A) E16.5 coronal sections of *Nectin1*$_{4402}$ H2B-RFP/*Nectin4*$_{2589}$ H2B-YFP PS immunostained with GFP (green) and mCherry (red), demonstrating rare dual-transduced cells (yellow arrows in high magnification image of boxed region, below). (B) Immunofluorescent image of E14.5 *Nectin1*$_{4402}$;*Nectin4*$_{2589}$ and WT PS stained with nectin-1 (red), nectin-4 (green) and H2B-RFP. Cells transduced with the double shRNA construct show efficient loss of both nectin-1 and nectin-4. (C) E16.5 *Nectin1*$_{4402}$;*Nectin4*$_{2589}$ oral cavity immunostained for K14 (green) and H2B-RFP (red) showing K14+ epithelia within the palatal mesenchyme. Zoomed region (greyscale K14 image) highlighted by yellow dashed box above. (D) Immunofluorescent image of E14.5 *Nectin1*$_{4402}$;*Nectin4*$_{2589}$ and WT littermate demonstrating delays in PS elevation. (E) Zoom of yellow boxed region in (D) showing direct contact between transduced H2B-RFP+ (red) cells of the PS and lateral tongue with gap in K8+ (grey) periderm layer, suggesting possible intraoral adhesion. Scale bars 100 μm (A), 50μm (B,E), 1 mm (C; large), 0.5 mm (C; zoom), 200 μm (D).* $P < 0.05$, ** $P < 0.01$, *** $P < 0.001$, by Fisher's exact test.